A Comparison of Kriging and Cokriging for Estimation of Underwater Acoustic Communication Performance

George P. Kontoudis
Virginia Tech
Blacksburg, VA, USA
gpkont@vt.edu

Daniel J. Stilwell
Virginia Tech
Blacksburg, VA, USA
stilwell@vt.edu

ABSTRACT

Mobile underwater communication network nodes, such as autonomous underwater vehicles, can use estimates of underwater acoustic communication performance to anticipate where they are likely to be connected to the communication network. In this paper, we consider the challenge of estimating a spatial field that represents underwater acoustic communication performance from a set of measurements. Kriging, which is widely used in geostatistics, has been previously used to estimate the communication performance at unknown locations, by performing spatial extrapolation. We compare kriging to cokriging where the latter is a bivariate estimation method. The methodology yields estimates of communication performance at desired locations based on measurements acquired at other locations. Moreover, a variance measure is provided that characterizes the uncertainty of the estimation. We present the structure of the proposed estimation technique and its computational complexity. We evaluate the efficacy of the technique by considering an approximate linear-log model of the communication performance, environmental noise, and a direct comparison of kriging and cokriging results. We provide two sets of simulations in which the proposed multivariate cokriging framework outperforms the univariate kriging in the estimation process.

CCS CONCEPTS

• **Networks** → **Network performance modeling**; • **Computer systems organization** → *Robotic autonomy*; • **Mathematics of computing** → *Multivariate statistics.*

KEYWORDS

communication performance, spatial estimation, underwater robots, acoustics, multivariate kriging

ACM Reference Format:
George P. Kontoudis and Daniel J. Stilwell. 2019. A Comparison of Kriging and Cokriging for Estimation of Underwater Acoustic Communication Performance. In *WUWNet '19: ACM International Conference on Underwater Networks & Systems, October 23–25, Atlanta, GA, USA.* ACM, New York, NY, USA, 8 pages. https://doi.org/10.1145/nnnnnnn.nnnnnnn

WUWNet '19, October 23–25, 2019, Atlanta, GA

ACM ISBN 978-x-xxxx-xxxx-x/YY/MM…$15.00
https://doi.org/10.1145/nnnnnnn.nnnnnnn

1 INTRODUCTION

Coordination of multiple autonomous agents requires effective communication. For agents that operate underwater, inter-vehicle communication is usually accomplished using acoustic signals. The performance of communication does not depend only to the range of the vehicles, but also to the environment. For example, autonomous underwater vehicles (AUV) may operate to highly varying environments that include variability in depth, water density, sea state, shipping noise, and turbulence [15]. Efficient communication can be used to improve navigation accuracy and localization [17]. Accurate estimates of anticipated communication performance can be exploited to plan better utilization of communication resources and conserve energy. Our focus in this work is on investigating stochastic acoustic communication performance estimation for applications with mobile communication nodes, such as autonomous underwater vehicles. Our general approach may be applicable to other domains, including aerial and ground communication using radio frequency signals.

Related work: Underwater communications is usually achieved with acoustic signals. A survey of prospects and problems in underwater acoustic communications is documented in [11]. A distributed kriging methodology was used in [19] to estimate coverage holes in large-scale wireless sensor networks. Horner *et al.* [8], proposed a methodology, based partially on kriging, to generate local and global acoustic communication performance maps. The authors in [23] developed a cooperative robust algorithm to compose a spatial map of underwater acoustic communication signals and channel parameters, using an H_∞ filter and kriging. In [18], the acoustic communication performance of micro autonomous underwater vehicles was assessed with an experimental process. The results reveal that for non-stationary transmission, i.e. moving vehicle, several factors reduce the communication performance, including multi-path effect of acoustic transmission, path hopping, and the Doppler effect. In [16], a methodology that combines kriging and compressive sensing methods [2], namely kriged compressive sensing (KCS), was utilized to reconstruct acoustic intensity fields. More specifically, KCS uses ordinary kriging to estimate the acoustic intensity field in unsampled locations and its variance to weigh the importance of the estimated values. Then, by using compressive sensing, the authors construct the spatial map with sparse data. However, kriging is a univariate spatial estimation technique, i.e. employs one variable, and ignores other variables that may improve the estimation accuracy.

The inverse problem of estimating the acoustic communication performance at a given location is the estimation of location given the communication performance. For the case of WiFi in air, the objective is to estimate the location of a vehicle based on wireless

received signal strength. In [7], the authors employed Gaussian processes to determine a likelihood model of received signal strength and estimate the location of robots. This approach demands a training set of received signal strength observations compared with a ground truth map, that is computationally expensive for large maps. Therefore, the authors in [6] proposed a Gaussian process latent variable model to generate wireless signal strength maps and solve the WiFi SLAM. The Gaussian process framework is closely related with kriging [22], yet kriging is restricted to small variable spaces.

Contributions: The contribution of this paper is twofold. First, we formulate an approximate communication performance model that takes into account the environmental conditions. We use this model to motivate our specific approach to kriging, and to generate numerical simulations of communication performance that were used to exercise our framework. Next, we propose a bivariate approach to estimate the communication performance between two vehicles in a time-varying environment, by using cokriging.

Notation: The notation here is standard. The set of real numbers is denoted $\mathbb{R}$, the set of all positive real numbers $\mathbb{R}^+$, the set of all positive real numbers including zero $\mathbb{R}_{\geq 0}$, the set of $n \times m$ real matrices $\mathbb{R}^{n\times m}$, and the set of natural numbers $\mathbb{N}$. The transpose and inverse operators are denoted $(\cdot)^\intercal$ and $(\cdot)^{-1}$ respectively. The $|K|$ denotes the cardinality of the set K. The p-norm of a vector is denoted $\|\cdot\|_p$ and the power summation $\oplus$.

Structure: The remainder of this paper is structured as follows. Section 2 formulates the problem, Section 3 focuses on the spatial estimation techniques, Section 4 presents the estimation framework, Section 5 presents the results and the simulations, and Section 6 concludes the paper and provides future directions.

2 PROBLEM FORMULATION

In this section we present the measurement model of the vehicles and we discuss the physical process of the environment. We also assess the acoustic communication performance with a signal-to-noise ratio (SNR) model of the sonar.

2.1 Communication Performance

The measurement model of all agents is identical and described by,

$$Y_i(\mathbf{x}; t) = Z(\mathbf{x}; t) + \epsilon, \tag{1}$$

where $Y_i(\mathbf{x}; t)$ is the measurement of communication performance of agent i at spatial locations $\mathbf{x} = [x \quad y]^\intercal \in \mathbb{R}^2$, $Z(\mathbf{x}; t)$ represents the random field, and $\epsilon \sim (0, \sigma_Y^2)$ is a zero-mean Gaussian noise.

We seek a simple model of underwater acoustic communication performance. We employ the passive sonar equation that models direct communication between the transmitter and the receiver [5, 9]. Unlike an active sonar model, we do not consider interaction with a target system e.g., reverberation noise. Since we are interested in applications with relatively slow-moving AUVs, we ignore frequency shifting and spreading that are due to motion-induced Doppler effect.

To approximate the communication performance between two agents we use the SNR. In principle, the higher the SNR, the more likely is to detect the transmitted signal. The passive sonar equation is expressed,

$$\text{SNR} = \text{SL} - \text{TL} - \text{NL} + \text{DI}, \tag{2}$$

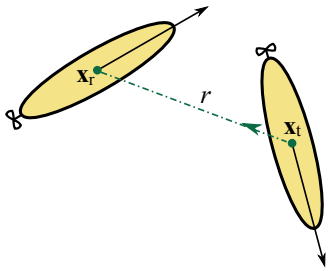

Figure 1: An acoustic communication scenario of two underwater vehicles at range r. The transmitting vehicle is located at position $\mathbf{x}_\text{t}$ and the receiving vehicle at position $\mathbf{x}_\text{r}$.

where SL is the source level, TL is the transmission loss, NL is the noise level, and DI is the directivity index. In practice, the source level is provided by the manufacturer of the transmitter and we assume that the effect of the directivity index is negligible, similarly to [13]. The transmission loss can be computed as,

$$\text{TL}(r) = \text{TL}_\text{sph}(r) - \text{TL}_\text{a}(r), \tag{3}$$

where TL_sph is the spherical spreading loss, TL_a is the attenuation, and $r = \|\mathbf{x}_\text{r} - \mathbf{x}_\text{t}\|_2$ is the range of two vehicles. In Fig. 1 we illustrate the case of acoustic communication between two underwater vehicles at range r, with $\mathbf{x}_\text{t}$ the position of the *transmitting* vehicle and $\mathbf{x}_\text{r}$ the position of the *receiving* vehicle. Spherical spreading loss is proportional to the log of range, $\text{TL}_\text{sph}(r) = 20 \log r$. Attenuation depends on the signal frequency due to the process of transferring the acoustic energy into heat. More specifically, for a signal frequency of $f = 25$ kHz the absorption coefficient is $a = 5.56$ dB/km [1]. Thus, (3) results in a linear-log relationship,

$$\text{TL}(r) = 20 \log r - 0.00556r. \tag{4}$$

2.2 Environmental Conditions

In our simplified communication model, we capture various environmental effects, such as multi-path, density gradients, etc, as simply noise that reduces the SNR. The noise comprises of ambient noise, transient noise, and self-noise [5].

Sources of ambient noise include the shipping and sea state. Ambient noise is approximated by the Wenz curves [21],

$$\text{NL}_\text{amb} = \text{NL}_\text{ship} \oplus \text{NL}_\text{SS}, \tag{5}$$

where NL_ship is the shipping noise and NL_SS is the sea state noise. The power summation operator for L_k elements, with $k = 1, \ldots, N_k$, is given by $\oplus = 10 \log \sum_{k=1}^{N_k} 10^{L_k/10}$. For a signal frequency of $f = 25$ kHz the shipping noise is almost zero, as $\text{NL}_\text{SS} \gg \text{NL}_\text{ship}$. To this end, (5) simplifies to $\text{NL}_\text{amb} = \text{NL}_\text{SS}$.

Subsequently, if we neglect the transient noise (e.g, biological organisms) and self-noise the communication performance yields,

$$\text{SNR} = \text{SL} - 20 \log r + 0.00556r - \text{NL}_\text{SS}. \tag{6}$$

Remark 1. *Since the communication signal transmits in high frequency ($f = 25$ kHz), the transient noise can be neglected. Similarly, the cavitation noise of the propeller vanishes. However, the flow noise—which is produced by the propeller—may affect the source level of the transmitted signal and/or the received signal strength. In fact, this*

will lead to anisotropic SNR, depending not only on the position but also on the orientation of the vehicle. In this work, we do not consider anisotropic sensing.

3 MULTIVARIATE SPATIAL ESTIMATION

In this section, we introduce kriging, a spatial estimation technique that estimates values at locations of interest, based on measurements from other locations. First, we discuss the ordinary kriging (OK) and then we present the multivariate kriging, namely cokriging (COK).

Let us first introduce some basic notions of the random fields. A comprehensive discussion on the topic can be found in [4]. Let $Z(\mathbf{x})$ be a *random field* with a positive-definite covariance matrix $\mathrm{Cov}(Z(\mathbf{x}_1), Z(\mathbf{x}_2)) \succ 0$ for all $\mathbf{x} \in \mathbb{R}^2$. The semivariogram with constant mean $\mathrm{E}\{Z(\mathbf{x})\} = \mu$ is defined,

$$\gamma(\mathbf{x}_1, \mathbf{x}_2) \coloneqq \frac{1}{2}\,\mathrm{E}\{(Z(\mathbf{x}_1) - Z(\mathbf{x}_2))^2\}. \tag{7}$$

The random field is *intrinsically stationary* if $\mathrm{Cov}(Z(\mathbf{x}_1), Z(\mathbf{x}_2)) = C(\mathbf{x}_1 - \mathbf{x}_2)$ for all $\mathbf{x} \in \mathbb{R}^2$ and the function $C(\cdot)$ is called *covariogram*. An intrinsically stationary random field with a constant mean is called *second-order stationary*. Moreover, if $C(\mathbf{x}_1 - \mathbf{x}_2)$ is only a function of the Euclidean norm $\|\mathbf{x}_1 - \mathbf{x}_2\|_2$, then the covariogram is *isotropic*. The correlogram is defined,

$$\rho(\mathbf{x}) \coloneqq \frac{C(\mathbf{x})}{C(0)}, \tag{8}$$

where $C(0) = \mathrm{Var}\{Z(\mathbf{x})\}$ is the *sill* and the data is normalized so that it has zero mean an unit variance (see (37)). For a second-order stationary random field with normalized measurements and $\|\mathbf{x}_1 - \mathbf{x}_2\|_2 = h$, the semivariogram is the mirror image of the covariance, resulting,

$$\gamma(h) = 1 - C(h). \tag{9}$$

Next, we present fundamental notions of the multivariate case [20]. In multivariate statistics the covariance comprises of direct and cross-covariance functions. The *joint second-order* hypothesis assumes a constant mean for every variable,

$$\mathrm{E}\{Z_j(\mathbf{x})\} = \mu_j, \tag{10}$$

and a cross-covariance function in the form,

$$\mathrm{E}\{(Z_j(\mathbf{x}_1) - \mu_i)(Z_l(\mathbf{x}_2) - \mu_l)\} = C_{jl}(h). \tag{11}$$

The cross-covariance function C_{jl} captures the variation of variables over distance. The *joint intrinsic model* imposes the cross-variogram structure,

$$\gamma_{jl}(\mathbf{x}_1, \mathbf{x}_2) = \frac{1}{2}\,\mathrm{E}\{(Z_j(\mathbf{x}_1) - Z_j(\mathbf{x}_2))(Z_l(\mathbf{x}_1) - Z_j(\mathbf{x}_2))\}. \tag{12}$$

That is, the cross-variogram measures the difference of variances over distance. Furthermore, the cross-correlogram, by assuming the *intrinsic correlation model*, is expressed,

$$\rho_{jl}(h) = \frac{C_{jl}(h)}{C_j(0)C_l(0)}, \tag{13}$$

where $C_j(0) = \mathrm{Var}\{Z_j(\mathbf{x})\}$, $C_l(0) = \mathrm{Var}\{Z_l(\mathbf{x})\}$ are the sills where for normalized measurements $C_j(0) = C_l(0) = 1$.

3.1 Ordinary Kriging

Let us now describe the ordinary kriging technique. We consider multiple measurements at locations $\mathbf{x}_j \in \mathbb{R}^2$, $j = 1, \ldots, M$ with $M \in \mathbb{N}$. In ordinary kriging the measurements are modeled as,

$$Z(\mathbf{x}) = \mu + \nu(\mathbf{x}), \tag{14}$$

where $Z(\mathbf{x}) \in \mathbb{R}$ is a second-order stationary random field, $\mu \in \mathbb{R}$ is the unknown constant mean that represents the large scale variation, and $\nu(\mathbf{x})$ is the zero-mean Gaussian field that captures the small scale variability. We are interested in estimating the mean value of the random field at an unmeasured location $\mathbf{x}_0$, based on the measured data $Z(\mathbf{x})$. We use a linear unbiased estimator,

$$\begin{aligned}\hat{Z}(\mathbf{x}_0) &= \sum_{j=1}^{N_j} \beta_j Z(\mathbf{x}_j) + (1 - \sum_{j=1}^{N_j} \beta_j)\mu \\ &= \boldsymbol{\beta}^\intercal \mathbf{Z}(\mathbf{x}),\end{aligned} \tag{15}$$

where $\boldsymbol{\beta} = [\beta_1 \ \ldots \ \beta_{N_j}]^\intercal \in \mathbb{R}^{N_j}$ are the weights we seek to obtain. The unbiasedness of the estimator $\sum_{j=1}^{N_j} \beta_j = 1$ relaxes the assumption of a known global mean μ. As a result, we can perform kriging with the measurements and not its residuals, $Z(\mathbf{x}_j) - \mu$. Next, we formulate the unconstrained minimization problem with a Lagrange multiplier λ_{OK} to include the unbiasedness constraint. The solution to the minimization problem results in,

$$\boldsymbol{\beta}_{\mathrm{OK}} = \boldsymbol{\Gamma}_{\mathrm{OK}}^{-1} \boldsymbol{\gamma}_{\mathrm{OK}}, \tag{16}$$

where $\boldsymbol{\beta}_{\mathrm{OK}} = [\boldsymbol{\beta}^\intercal \ \lambda_{\mathrm{OK}}]^\intercal \in \mathbb{R}^{N_j+1}$ is a vector that contains the weights $\boldsymbol{\beta}$ and the Lagrange multiplier λ_{OK}. The non-singular matrix $\boldsymbol{\Gamma}_{\mathrm{OK}} \in \mathbb{R}^{(N_j+1)\times(N_j+1)}$ considers the *redundancy* of measurements and is given by,

$$\boldsymbol{\Gamma}_{\mathrm{OK}} = \begin{bmatrix} \gamma(\mathbf{x}_1, \mathbf{x}_1) & \ldots & \gamma(\mathbf{x}_1, \mathbf{x}_N) & 1 \\ \vdots & \ddots & \vdots & \vdots \\ \gamma(\mathbf{x}_N, \mathbf{x}_1) & \ldots & \gamma(\mathbf{x}_N, \mathbf{x}_N) & 1 \\ 1 & \ldots & 1 & 0 \end{bmatrix} \coloneqq \begin{bmatrix} \boldsymbol{\Gamma} & \mathbf{1} \\ \mathbf{1}^\intercal & 0 \end{bmatrix}, \tag{17}$$

where $\mathbf{1} \in \mathbb{R}^{N_j}$ is a vector of ones. The vector $\boldsymbol{\gamma}_{\mathrm{OK}} \in \mathbb{R}^{(N_j+1)}$ takes into account the *closeness* of the measurements to the location of interest $\mathbf{x}_0$ and yields,

$$\boldsymbol{\gamma}_{\mathrm{OK}} = \begin{bmatrix} \gamma(\mathbf{x}_0, \mathbf{x}_1) \\ \vdots \\ \gamma(\mathbf{x}_0, \mathbf{x}_N) \\ 1 \end{bmatrix} \coloneqq \begin{bmatrix} \boldsymbol{\gamma}_0 \\ 1 \end{bmatrix}. \tag{18}$$

The unique solution of (16) yields the vector of unknown weights,

$$\boldsymbol{\beta} = \boldsymbol{\Gamma}^{-1}\Big(\boldsymbol{\gamma}_0 - \mathbf{1}\lambda_{\mathrm{OK}}\Big), \tag{19}$$

and the Lagrange multiplier,

$$\lambda_{\mathrm{OK}} = \frac{\mathbf{1}^\intercal \boldsymbol{\Gamma}^{-1} \boldsymbol{\gamma}_0 - 1}{\mathbf{1}^\intercal \boldsymbol{\Gamma}^{-1} \mathbf{1}}, \tag{20}$$

Sequentially, the weights $\boldsymbol{\beta}$ and the Lagrange multiplier λ_{OK} can be used for the computation of the ordinary kriging variance as,

$$\sigma^2_{\mathrm{OK}}(Z(\mathbf{x}_0)) = \mathrm{Var}_{\mathrm{OK}}\{Z(\mathbf{x}_0)\} = \boldsymbol{\beta}^\intercal \boldsymbol{\gamma}_0 + \lambda_{\mathrm{OK}}. \tag{21}$$

In terms of the covariance matrix for normalized measurements, we use (9) and the solution follows accordingly.

3.2 Multicollocated Ordinary Cokriging

In this section we shall describe the multicollocated ordinary cokriging (MCOK). We observe in (6) that our simplified model of communication performance is a linear-log function of the range of the vehicles. Moreover, the range measurements are acquired simultaneously with the SNR. Interestingly, there exists a spatial correlation of these two variables. For instance, when we seek to estimate the communication performance at a specific location, the range of the vehicles is critical. In case that the vehicles navigate in close proximity, then the communication performance is expected be high. On the contrary, in case that the vehicles have large range, then the communication signal will be degraded and corrupted by noise. Therefore, we want to estimate the communication performance at a specific location for a given range.

Cokriging is the multivariate kriging that augments the estimation process with the covariances and cross-covariances of the variables involved in the process [20]. The key idea underlying this work is to use the range of the vehicles as a secondary variable in cokriging in order to improve the SNR estimation. Thus, we incorporate two variables: i) the communication performance as the primary variable and ii) the range of the vehicles as the secondary variable. The ordinary cokriging estimator for two variables yields,

$$\begin{aligned}\hat{Z}(\mathbf{x}_0) &= \sum_{j=1}^{N_j} \beta_{j,1} Z_1(\mathbf{x}_j) + \sum_{l=1}^{N_l} \beta_{l,2} Z_2(\mathbf{x}_l) \\ &= \boldsymbol{\beta}_{\mathrm{COK},1}^{\intercal} \mathbf{Z}_1(\mathbf{x}) + \boldsymbol{\beta}_{\mathrm{COK},2}^{\intercal} \mathbf{Z}_2(\mathbf{x}),\end{aligned} \tag{22}$$

where $\boldsymbol{\beta}_{\mathrm{COK},1} = [\beta_{1,1}, \ldots, \beta_{N_j,1}]^{\intercal}$, $\boldsymbol{\beta}_{\mathrm{COK},2} = [\beta_{1,2}, \ldots, \beta_{N_l,2}]^{\intercal}$ are the stacked vectors of the unknown weights of two variables, $\mathbf{Z}_1 \in \mathbb{R}^{N_j}$ and $\mathbf{Z}_2 \in \mathbb{R}^{N_l}$ with $N_l > N_j$ are the stacked vectors of the measurements of the two variables at locations $\mathcal{X}_{\mathrm{pr}} = \{\mathbf{x}_j\}_{j=1}^{N_j}$ and $\mathcal{X}_{\mathrm{sec}} = \{\mathbf{x}_l\}_{l=1}^{N_l}$ respectively. The unbiasedness of the estimator for the primary variable $\mathbf{1}^{\intercal}\boldsymbol{\beta}_{\mathrm{COK},1} = 1$ and for the secondary variable $\mathbf{1}^{\intercal}\boldsymbol{\beta}_{\mathrm{COK},2} = 0$, relaxes the assumption of known global means. Therefore, we implement cokriging with the measurements and not its residuals. Then, we formulate the unconstrained minimization problem with two Lagrange multipliers to account for the unbiasedness constraints $\lambda_{\mathrm{COK},1}$, $\lambda_{\mathrm{COK},2}$. The solution to the minimization problem results in the system of linear equations,

$$\boldsymbol{\beta}_{\mathrm{COK}} = \boldsymbol{\Gamma}_{\mathrm{COK}}^{-1} \boldsymbol{\gamma}_{\mathrm{COK}}, \tag{23}$$

where $\boldsymbol{\beta}_{\mathrm{COK}} = [\boldsymbol{\beta}_{\mathrm{COK},1}^{\intercal}\ \boldsymbol{\beta}_{\mathrm{COK},2}^{\intercal}\ \lambda_{\mathrm{COK},1}\ \lambda_{\mathrm{COK},2}]^{\intercal} \in \mathbb{R}^{N_j+N_l+2}$ is the unknown vector we seek to obtain. The non-singular matrix $\boldsymbol{\Gamma}_{\mathrm{COK}} \in \mathbb{R}^{(N_j+N_l+2)\times(N_j+N_l+2)}$ captures the measurement redundancy and has the form of,

$$\boldsymbol{\Gamma}_{\mathrm{COK}} = \begin{bmatrix} \boldsymbol{\Gamma}_1 & \boldsymbol{\Gamma}_{12} & \mathbf{1} & \mathbf{0} \\ \boldsymbol{\Gamma}_{21} & \boldsymbol{\Gamma}_2 & \mathbf{0} & \mathbf{1} \\ \mathbf{1}^{\intercal} & \mathbf{0}^{\intercal} & 0 & 0 \\ \mathbf{0}^{\intercal} & \mathbf{1}^{\intercal} & 0 & 0 \end{bmatrix}. \tag{24}$$

The vector $\boldsymbol{\gamma}_{\mathrm{COK}} \in \mathbb{R}^{(N_j+N_l+2)}$ considers the closeness of the measurements to the location of interest and leads to,

$$\boldsymbol{\gamma}_{\mathrm{COK}} = \begin{bmatrix} \boldsymbol{\gamma}_{\mathbf{0},1} \\ \boldsymbol{\gamma}_{\mathbf{0},12} \\ 1 \\ 0 \end{bmatrix}. \tag{25}$$

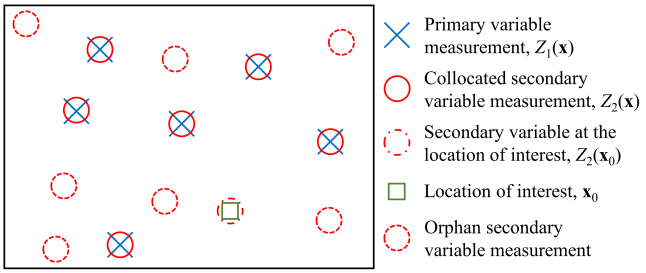

Figure 2: The multicollocated setup. The primary variable measurements $Z_1(\mathbf{x})$ are shown in blue x-marks, the collocated secondary variable measurements $Z_2(\mathbf{x})$ are depicted with red solid circles, the secondary variable measurement at the location of interest $Z_2(\mathbf{x}_0)$ is shown in red dash-dotted line, and the location of interest $\mathbf{x}_0$ is presented with a green rectangular. The dashed red circle represent the orphan secondary variable measurements $\mathcal{X}_{\mathbf{orp}}$ that are not used in the multicollocated cokriging.

In general, the practical challenges with cokriging are: i) the modeling of all covariances and cross-covariances, ii) all covariances and cross covariances jointly need to be positive definite, and iii) the solution generates very large linear systems, i.e. $(N_j + N_l + 2)$-equations. For these reasons, we employ the multicollocated cokriging which accounts for: i) all primary variable measurements, ii) all secondary variable measurements at the locations of the primary variable measurements, and iii) the secondary variable measurement at the location of interest, as shown in Fig. 2. The orphan secondary variable measurements $\mathcal{X}_{\mathrm{orp}} = \mathcal{X}_{\mathrm{pr}} \backslash \mathcal{X}_{\mathrm{sec}}$, i.e. not collocated with primary variable measurements, are not used in this framework. The multicollocated cokriging model (or Markov Model 2) has been proven to be necessary and sufficient for cokriging in the stationary case [10, 12]. Next, we introduce the Markov screening and the Bayesian updating assumptions.

Assumption 1 (Markov Screening). *The primary variable Z_1 at any location $\boldsymbol{x}_1$ depends conditionally only on the secondary variable Z_2 at location $\boldsymbol{x}_1$, screening out the influence of the secondary variable Z_2 at any other location $\boldsymbol{x}_2$, which yields,*

$$\mathrm{E}\{Z_1(\boldsymbol{x}_1) \mid Z_2(\boldsymbol{x}_1), Z_2(\boldsymbol{x}_2)\} = \mathrm{E}\{Z_1(\boldsymbol{x}_1) \mid Z_2(\boldsymbol{x}_1)\}. \tag{26}$$

Assumption 2 (Bayesian Updating). *The primary and the secondary variables are linearly related through the correlation coefficient $\rho_{12}(0)$ at any location, which yields,*

$$\mathrm{E}\{Z_1(\boldsymbol{x}) \mid Z_2(\boldsymbol{x})\} = \rho_{12}(0) Z_2(\boldsymbol{x}). \tag{27}$$

From Assumption 1 and Assumption 2 the cross-correlogram takes the form,

$$\rho_{12}(\mathbf{h}) = \rho_{12}(0)\rho_2(\mathbf{h}), \tag{28}$$

which in terms of covariogram yields,

$$\gamma_{12}(\mathbf{h}) = p\gamma_2(\mathbf{h}), \tag{29}$$

where $p = \rho_{12}(0)\sigma_1/\sigma_2$ is the slope of the linear regression with σ_1, σ_2 the standard deviations of the primary and secondary variables respectively. Note that if the measurements are normalized with respect to the variance, then $p = \rho_{12}$ and subsequently $\sigma_1 = \sigma_2 = 1$.

Next, we consider a regression model of the primary variable on the secondary variable in the form,

$$Z_1(\mathbf{x}) = pZ_2(\mathbf{x}) + R(\mathbf{x}), \tag{30}$$

where $R(\mathbf{x})$ is the orthogonal residual which can also be considered as $R(\mathbf{x}) = Z_1(\mathbf{x}) - pZ_2(\mathbf{x})$. Note that since $Z_1(\mathbf{x})$ and $Z_2(\mathbf{x})$ are Gaussian, $R(\mathbf{x})$ is also Gaussian.

Assumption 3 (Residual Independence). *The residual $R(\boldsymbol{x})$ is an independent random function of the secondary variable at any location, which yields,*

$$\mathrm{Cov}(R(\boldsymbol{x}), Z_2(\boldsymbol{x})) = 0. \tag{31}$$

Due to Assumption 3, the linear regression (30) maintains the *homoscedasticity* properties of kriging, i.e. the variance of the primary variable can be computed at locations of interest, without actual measurement of the primary variable at this location.

The orthogonal residual can be computed with the ordinary kriging as discussed in Subsection 3.1 with a linear unbiased estimator in the form,

$$\hat{R}(\mathbf{x}_0) = \boldsymbol{\beta}_{\mathrm{R}}^{\mathsf{T}} R(\mathbf{x}), \tag{32}$$

where $\boldsymbol{\beta}_{\mathrm{R}}$ are the residual corresponding weights of the ordinary kriging. Note that the domain of measurements for the ordinary kriging of the orthogonal residual, does not include the location of interest $\mathcal{D}_{\mathrm{x}} = \mathcal{X}_{\mathrm{pr}} \cup \mathcal{X}_{\mathrm{sec}} \not\ni \mathbf{x}_0$. Then, we use the residual variogram function γ_{R} to construct the covariance of the primary variable as,

$$\gamma_1(h) = p^2\gamma_2(h) + \gamma_{\mathrm{R}}(h). \tag{33}$$

The rest elements of the non-singular matrix $\boldsymbol{\Gamma}_{\mathrm{MCOK}}$ result from (29) and the experimental variogram of the secondary variable. The multicollocated ordinary cokriging estimator for two variables yields,

$$\begin{aligned}\hat{Z}_1(\mathbf{x}_0) &= pZ_2(\mathbf{x}_0) + \hat{R}(\mathbf{x}_0) \\ &= \sum_{j=1}^{N_j} \beta_{\mathrm{R},j} Z_{1,j} + p\left(Z_2(\mathbf{x}_0) - \sum_{l=1}^{N_l-1} \beta_{\mathrm{R},l} Z_{2,l}\right).\end{aligned} \tag{34}$$

where $Z_2(\mathbf{x}_0)$ is the measurement of the secondary variable measurement at the location of interest and $N_j = |\mathcal{D}_{\mathrm{x}}|$. The corresponding variance yields,

$$\sigma^2_{\mathrm{MCOK}}(Z_1(\mathbf{x}_0)) = \mathrm{Var}_{\mathrm{MCOK}}\{Z_1(\mathbf{x}_0)\} = \mathrm{E}\{\hat{R}(\mathbf{x}_0) - R(\mathbf{x}_0)\}. \tag{35}$$

Remark 2. *The multicollocated cokriging estimation* (34) *does not require the cross-covariance function and also results in a significantly smaller system of equations. To this end, we just need to compute the ordinary kriging of the residual R that comprises of (N_j+1)-equations and retain the same properties of solving the ordinary cokriging that consists of $(N_j + N_l + 2)$-equations, with $N_l > N_j$. This constitutes a significant reduction in the computational effort of the proposed technique.*

Remark 3. *In Assumption 2 we considered a linear relation of the primary with the secondary variable. However, according to* (6) *the communication performance is linear-logarithmically related with the range of the vehicles. Therefore, we expect smoother estimation results than the ground truth values.*

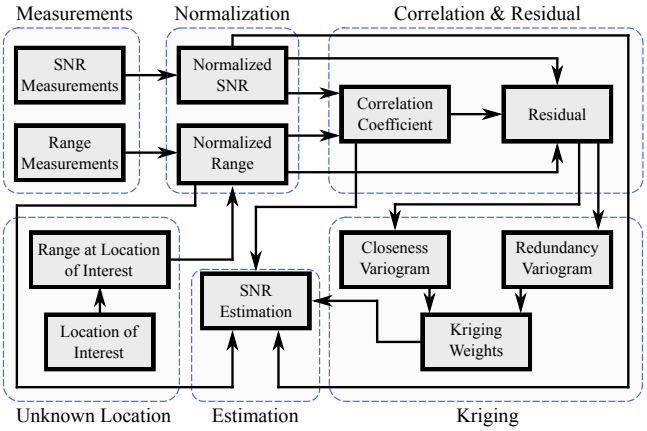

Figure 3: The structure of the communication performance estimator with multicollocated ordinary cokriging. The sequence operates clockwise, starting from the measurements. The structure incorporates six stages: 1) collection of measurements, 2) normalization of measurements, 3) computation of the correlation coefficient and the orthogonal residual, 4) ordinary kriging of the residual, and 5) the unknown location to 6) estimate the communication performance.

4 SPATIAL ESTIMATION FRAMEWORK

In this section, we discuss the structure of the proposed communication performance estimation with multicollocated cokriging and the computational complexity of both kriging and cokriging.

4.1 Estimation Structure

The multicollocated ordinary cokriging is shown in Fig. 3. The structure consists of collecting the measurements; normalizing the measurements; computing the correlation factor and the orthogonal residual; kriging the residual; and estimating the communication performance at the unknown location.

We start by collecting measurements of communication performance (SNR) and the range of the vehicles. SNR is the primary variable Z_1 and range the secondary Z_2. Then, we normalize the measurements with respect to the variance,

$$\tilde{Z}_{\delta,j} = \frac{Z_{\delta,j} - \mu_\delta}{\sqrt{\mathrm{Var}\{Z_\delta\}}}, \tag{36}$$

where we assume there are $j = 1, \ldots, N_j$ measurements. Primary measurements correspond to $\delta = 1$, secondary measurements correspond to $\delta = 2$, and $\mu_\delta = (1/N_j)\sum_{j=1}^{N_j} Z_{\delta,j}$ is the mean of the corresponding δ variable. This normalization results in a zero mean $\tilde{\mu}_\delta = 0$ and a variance $\mathrm{Var}\{\tilde{Z}_\delta\} = 1$ for both primary and secondary variable measurements. Thus, the slope of the linear regression in (29) matches the correlation coefficient, $p = \rho_{12}(0)$. Next, we compute the correlation coefficient $\rho_{12}(0)$ and the residual R as in (30). Then, we perform ordinary kriging to the residual to obtain the residual weights $\boldsymbol{\beta}_{\mathrm{R}}$ as in (19). An important aspect of kriging is

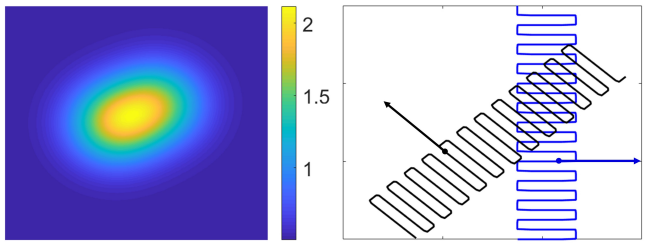

(a) (b)

Figure 4: The environmental conditions and the global path of the vehicles. (a) The spatial environmental conditions are modeled with a 2D Gaussian where higher mean values represent more corrupted SNR with noise. (b) The path of the first vehicle is shown with a black solid line and of the second vehicle with a blue solid line.

the variogram which in our case is modeled as a spherical function,

$$\gamma(h) = \begin{cases} C_1(0)\left(\frac{3}{2}\frac{h}{\alpha} - \frac{1}{2}\left(\frac{h}{\alpha}\right)^3\right) & , \ h < \alpha \\ C_1(0) & , \ h \geq \alpha, \end{cases} \tag{37}$$

where α is the kriging range and h the distance of the measurements. The kriging range represents the maximum distance of correlation between measurements. Thus, beyond the kriging range the measurements are considered uncorrelated. Finally, we employ the orthogonal residual weights, the normalized SNR measurements, the normalized range measurements, and the correlation coefficient to estimate the SNR at the location of interest and its variance as in (34), (35) respectively.

Remark 4. *The kriging range, the sill, and the nugget are user defined in our simulation environment, yet in practice should be experimentally identified. A robust methodology to fit variogram models with experimental data is discussed in [3].*

4.2 Computational Complexity

We discussed that ordinary cokriging can be reduced to ordinary kriging of the orthogonal residual in a multicollocated setup. Thus, instead of $O(N_j + N_l)^3$ computations for $\mathbf{\Gamma}^{-1}$ of ordinary cokriging (24), the proposed methodology requires $O(N_j)^3$ computations of ordinary kriging (17), where usually $N_l > N_j$. Next, if we consider the points of interest $\mathbf{P} = [\mathbf{x}_{0,1}, \ldots, \mathbf{x}_{0,P}] \in \mathbb{R}^{2\times P}$ to be approximately equal with the primary variable measurements $N_j = P$, then the multicollocated kriging results in complexity $O(N_j)^4$, while for the ordinary cokriging we would need $O(N_j+N_l)^4$ operations. Even though the multicollocated cokriging reduces the computational effort, it still remains intractable for online implementation with large number of measurements. To alleviate the online implementation, acceleration methods [14] may be used.

5 SIMULATIONS AND RESULTS

In this section, we provide simulations to compare the efficacy of the ordinary kriging to the proposed cokriging technique. We also present the communication performance between vehicles in a time-varying underwater environment.

5.1 Simulation Environment

The simulation environment captures the time-varying water conditions of the ambient noise with a 2D Gaussian. This is a common practice for the ambient noise, yet the mean of the Gaussian should not be zero [15]. Thus, the mean follows $\mu_{\text{amb}}(\mathbf{x}) = 0.3 + 1.2e^{-\|\mathbf{x}-[0.5\ \ 1]^\intercal\|^2} + e^{-\|\mathbf{x}-[1.5\ \ 1.5]^\intercal\|^2}$. We evaluated the mean over a grid of points in the space $\mathcal{S} := \mathbb{X}\times\mathbb{Y}$, where $\mathbb{X} = \{-2, -1.95, \ldots, 4\}$ and $\mathbb{Y} = \{-2, -1.95, \ldots, 3.95, 4\}$. The spatial environmental conditions as well as the global path of the vehicles are shown in Fig. 4. Based on the Wenz curves [21], typical ambient noise ranges $\text{NL}_{\text{amb}} \in [25, 45]$ dB, for signal frequency $f = 25$ kHz. The resulting mean for the space of interest outputs values $\mu_{\text{amb}}(\mathbf{x}) \in [0.50, 2.12]$. Thus, we assign ambient noise values to every cell, following a linear relation. For example, a cell with mean value $\mu_{\text{amb}}(\mathbf{x}) = 1.00$ results in ambient noise level,

$$\begin{aligned} \text{NL}_{\text{amb}}(\mathbf{x}) &= \text{NL}_{\text{amb}}^{\max} - \text{NL}_{\text{amb}}^{\min}\left(\frac{\mu_{\text{amb}}(\mathbf{x}) - \mu_{\text{amb}}^{\min}}{\mu_{\text{amb}}^{\max} - \mu_{\text{amb}}^{\min}}\right) \\ &= 45 - 25\left(\frac{1.00 - 0.50}{2.12 - 0.50}\right) = 37.28 \text{ dB}. \end{aligned}$$

The Wenz curves indicate ambient noise $\text{NL}_{\text{amb}} = 25$ dB for wind speed of less then 1 knot and $\text{NL}_{\text{amb}} = 45$ dB for wind speed of 28 to 33 knots. Therefore, the environment shown in Subfig. 4(a) is an extreme environment with high variations in wind speed that corrupt the SNR. The source level is chosen to be SL = 181 dB.

For the simulated measurements we need to evaluate the communication performance in the intermediate locations of the two vehicles. Thus, we introduce the evaluation path which is the straight line that connects the transmitting vehicle and the receiving vehicle. Next, we search for grid cells which accommodate the evaluation path and compute the average mean to assign an SNR value. Let the accommodating grid cells of the evaluation path to be $\mathcal{S}_{\text{x}} = \{\mu_{\text{amb}}(\mathbf{x}_1), \ldots, \mu_{\text{amb}}(\mathbf{x}_M)\} \subset \mathcal{S}$. Then, the resulting ambient noise is computed as $\text{NL}_{\text{amb}}(\mathbf{x}) = (1/M)\sum_{m=1}^{M}\mu_{\text{amb}}(\mathbf{x}_m)$. To this end, we not only consider the environmental conditions at the location of the transmitting $\mathbf{x}_{\text{t}}$ and the receiving vehicle $\mathbf{x}_{\text{r}}$, but also we acknowledge the environmental conditions of the path that the SNR propagates.

5.2 Communication Performance Estimation

We perform two sets of simulations focusing on the estimation of the communication performance with and without partial information of the environment with high ambient noise. We assume that the vehicles can acquire range measurements during all communication events.

In Fig. 5, we present the first set of simulations comprising of two scenarios with two vehicles following different paths. In the upper row of Fig. 5 the x–marks (black for vehicle 1 and red for vehicle 2) represent the 150 locations of measurements and the squares (gray for vehicle 1 and magenta for vehicle 2) the 283 unknown locations of interest. Note that in both cases we did not collect measurements from the area with increased ambient noise (depicted in the background with yellow). For the simulation shown in Fig. 5(a) we seek to assess communication performance when in the presence of ambient noise. T hat is significantly different from the measured communication performance, i.e. without any knowledge of the

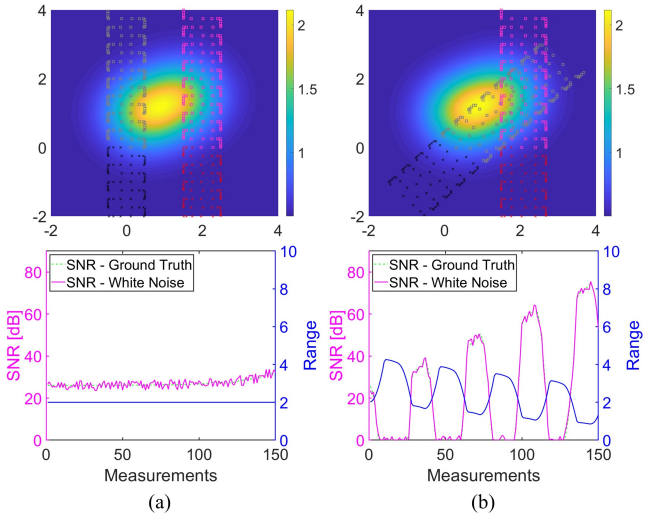

Figure 5: The first set of simulations with the vehicles paths and their corresponding measurements. (a) The vehicles follow similar zig-zag paths at the same direction and they collect 150 measurements right before the high-varying environment. (b) The vehicles follow opposite zig-zag paths at the same direction and they collect 150 measurements.

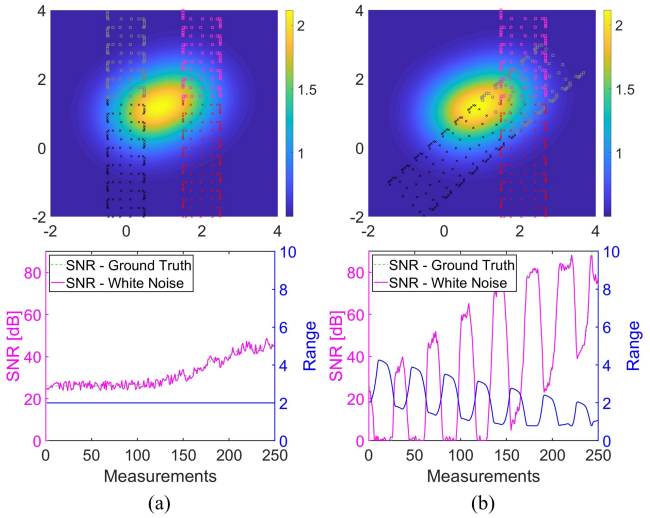

Figure 6: The second set of simulations with the vehicles paths and their corresponding measurements. (a) The vehicles follow similar zig-zag paths at the same direction and they collect 250 measurements including half of the the high-varying environment. (b) The vehicles follow opposite zig-zag paths at the same direction and they collect 250 measurements.

high variability of the environment. The corresponding SNR and range measurements are provided in the bottom row of Fig. 5. In Fig. 5(a), the vehicles follow similar zig-zag paths, and they are always facing in direction. As a result, the measurements are almost identical at all locations. The correlation coefficient of the normalized SNR and range measurements yields $\rho = -0.098$. In Fig. 5(b), the vehicles follow opposite zig-zag paths at different directions and the correlation coefficient is computed $\rho = -0.993$. Therefore, not only the measurements are highly varying, but also produce different amplitude. Since, in both cases the measurements were collected at a similar environment, the communication performance measurements are only affected by variations in range.

In Fig. 8, we show the absolute error of the SNR estimation with the ground truth of the ordinary kriging (OK) in red, and the multi-collocated ordinary cokriging (MCOK) in blue. The shaded areas represent the variation of the estimation and the dashed lines the mean of the absolute error. In the first case, OK and MCOK have identical estimation outcomes, yet for large indices which corresponding to being far from locations where measurements were acquired, the MCOK provides more reliable estimates. Also, the MCOK mean is slightly lower, 4.35% from the OK mean. The higher error values of both techniques from the first estimate to approximately the 160-th estimate indicates the high ambient noise in the center of the environment. In the second case, the OK estimates are more accurate at points of interest close to the last measurements, yet the error increases much faster for the OK estimates at distant locations of interest to the acquired measurements. Thus, MCOK outperforms in long-term estimates and its mean is significantly lower, 28.94% from the OK mean.

The second set of simulations is shown in Fig. 6. We consider two cases following identical paths with the previous set of simulations, but with more measurements to cover half of the high ambient noise area, appearing in the center of the environment. Our objective is to provide more measurements to both methodologies with information on the high ambient noise area of the environment. More specifically, we gather 250 measurements as illustrated in the upper row of Fig. 6 with black and red x-marks corresponding to vehicle 1 and vehicle 2 respectively. The unknown locations of interests are represented by gray and magenta squares corresponding to vehicle 1 and vehicle 2. The correlation coefficients result in $\rho = -0.064$ and $\rho = -0.957$ for the first and the second case respectively. Surprisingly, the second set of simulations provides insufficient results for both techniques with radially unbounded errors, even with more measurements, as presented in Fig. 8. In Fig. 8(a) the OK and MCOK provide sufficient estimates for locations of interest close to the last measurements, yet for distant locations of interest the estimation error is unsatisfactory. The MCOK produces lower mean error, 18.71% from the OK mean. In Fig. 8(b) both techniques show poor performance with high error measurements. Although, both techniques have unsatisfactory performance, the MCOK produces significantly lower mean in the order of 32.92% from the OK mean. The high absolute errors appear because ordinary kriging assumes constant means which consequently lead to locally biased kriging estimates.

In all cases the MCOK produces lower mean errors, revealing that the effect of the range is crucial to obtain better estimation results. Although in long-term estimates the MCOK provides more accurate results, in close proximity to the measurements the OK provides

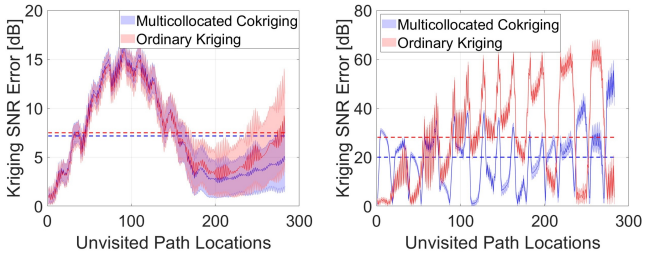

Figure 7: The absolute error values with their variance for the first set of simulations. The mean of the average error of the multicollocated cokriging and the ordinary kriging are illustrated in blue and red dashed lines respectively.

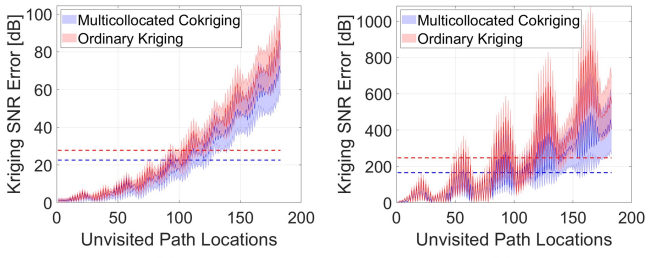

Figure 8: The absolute error values with their variance for the second set of simulations. Both approaches provide poor performance, yet the multicollocated cokriging outperforms the ordinary kriging estimates.

similar or even better results. In the second set of simulations both techniques demonstrate poor performance. This is occurred due to the nature of ordinary kriging that assumes a stationary constant mean, as discussed in (14). In practice, the spatial global mean is a conservative assumption, as usually the mean follows a *trend* over the spatial domain. An alternative kriging method with a non-stationary mean is the universal kriging, that considers basis functions to capture the underlying trend in the mean value.

6 CONCLUSION

Our work illustrates deficiencies in kriging for generating communication performance estimates, arising mainly from the structure of the assumptions. Moreover, our work shows that using range as a secondary variable in a cokriging formulation of the problem, yields lower absolute errors and performs better in long-term estimates. More specifically, we compare the proposed methodology with ordinary kriging and we show that the proposed framework provides better communication performance estimates with lower absolute errors in all simulation scenarios. Only in short-term estimates and in certain cases the ordinary kriging computes lower absolute errors. However, at distant locations of interest from the acquired measurements the proposed methodology provides better results. The simulations reveal that for realistic applications the assumption of stationary global mean of both techniques is rather conservative and develops unacceptable absolute errors.

Future work will focus on formulating and implementing an online, distributed communication performance estimation algorithm for underwater vehicles with anisotropic sensing. We will consider a nonlinear relation of the primary with the secondary variable. Moreover, we will conduct field trials to validate the efficacy of the estimation algorithm.

ACKNOWLEDGMENTS

This work was supported by the Office of Naval Research via grants N00014-18-1-2627 and N00014-19-1-2194.

REFERENCES

[1] Leonid M Brekhovskikh and Yu P Lysanov. 2001. *Fundamentals of ocean acoustics.* Springer.
[2] Emmanuel J Candes, Justin K Romberg, and Terence Tao. 2006. Stable signal recovery from incomplete and inaccurate measurements. *Communications on Pure and Applied Mathematics: A Journal Issued by the Courant Institute of Mathematical Sciences* 59, 8 (2006), 1207–1223.
[3] Noel Cressie. 1985. Fitting variogram models by weighted least squares. *Journal of the International Association for Mathematical Geology* 17, 5 (1985), 563–586.
[4] Noel Cressie. 1992. *Statistics for spatial data.* Wiley Online Library.
[5] Paul C Etter. 2018. *Underwater acoustic modeling and simulation.* CRC press.
[6] Brian Ferris, Dieter Fox, and Neil D Lawrence. 2007. WiFi-SLAM using Gaussian process latent variable models. In *International Joint Conferences on Artificial Intelligence*, Vol. 7. 2480–2485.
[7] Brian Ferris, Dirk Hähnel, and Dieter Fox. 2006. Gaussian processes for signal strength-based location estimation. In *Robotics: Science and Systems.*
[8] Douglas Horner and Geoffrey Xie. 2013. Data-driven acoustic communication modeling for undersea collaborative navigation. In *IEEE OCEANS-San Diego.* 1–10.
[9] Finn B Jensen, William A Kuperman, Michael B Porter, and Henrik Schmidt. 2011. *Computational ocean acoustics.* Springer Science & Business Media.
[10] Andre G Journel. 1999. Markov models for cross-covariances. *Mathematical Geology* 31, 8 (1999), 955–964.
[11] Liu Lanbo, Zhou Shengli, and Cui Jun-Hong. 2008. Prospects and problems of wireless communication for underwater sensor networks. *Wireless Communications and Mobile Computing* 8, 8 (2008), 977–994.
[12] Jacques Rivoirard. 2001. Which models for collocated cokriging? *Mathematical Geology* 33, 2 (2001), 117–131.
[13] Michael Shinego, Geoff Edelson, Francine Menas, Michael Richman, and Robert Nation. 2001. *Underwater Acoustic Data Communications for Autonomous Platform Command, Control and Communications.* Technical Report. BAE Systems and Technology.
[14] Balaji V Srinivasan, Ramani Duraiswami, and Raghu Murtugudde. 2010. Efficient kriging for real-time spatio-temporal interpolation. In *Conference on Probability and Statistics in the Atmospheric Sciences.*
[15] Milica Stojanovic and James Preisig. 2009. Underwater acoustic communication channels: Propagation models and statistical characterization. *IEEE Communications Magazine* 47, 1 (2009), 84–89.
[16] Jie Sun, Jiancheng Yu, Aiqun Zhang, Aijun Song, and Fumin Zhang. 2018. Underwater acoustic intensity field reconstruction by Kriged compressive sensing. In *ACM International Conference on Underwater Networks & Systems.* 5:1–5:8.
[17] Hwee-Pink Tan, Roee Diamant, Winston KG Seah, and Marc Waldmeyer. 2011. A survey of techniques and challenges in underwater localization. *Ocean Engineering* 38, 14-15 (2011), 1663–1676.
[18] Qiu-Yang Tao, Yue-Hai Zhou, Feng Tong, Ai-Jun Song, and Fumin Zhang. 2018. Evaluating acoustic communication performance of micro autonomous underwater vehicles in confined spaces. *Frontiers of Information Technology and Electronic Engineering* 19, 8 (2018), 1013–1023.
[19] Muhammad Umer, Lars Kulik, and Egemen Tanin. 2010. Spatial interpolation in wireless sensor networks: Localized algorithms for variogram modeling and Kriging. *Geoinformatica* 14, 1 (2010), 101.
[20] Hans Wackernagel. 2013. *Multivariate geostatistics: An introduction with applications.* Springer Science & Business Media.
[21] Gordon M Wenz. 1962. Acoustic ambient noise in the ocean: Spectra and sources. *The Journal of the Acoustical Society of America* 34, 12 (1962), 1936–1956.
[22] Christopher KI Williams and Carl E Rasmussen. 1996. Gaussian processes for regression. In *Advances in Neural Information Processing Systems.* 514–520.
[23] Wencen Wu, Aijun Song, Paul Varnell, and Fumin Zhang. 2014. Cooperatively mapping of the underwater acoustic channel by robot swarms. In *ACM International Conference on Underwater Networks and Systems.* 20:1–20:8.